Deriving connectivity from spiking activity in biophysical cortical microcircuits

Faraz Moghbel[1,2], Muhammad Taaha Hassan[1], Alexandre Guet-McCreight[1] and Etay Hay[1,2,3*]

[1] Krembil Centre for Neuroinformatics, Centre for Addiction and Mental Health, Toronto, ON M5T 1R8, Canada
[2] Department of Physiology, University of Toronto, Toronto, ON M5S 1A1, Canada
[3] Department of Psychiatry, University of Toronto, Toronto, ON M5S 1A1, Canada
*Correspondence: etay.hay@camh.ca

Abstract

Inferring detailed cortical microcircuit connectivity is essential for uncovering how information is processed in the brain. A common method *in vivo* uses short-lag spike cross-correlations to derive putative monosynaptic connections between pairs of neurons, but previous studies did not address confounds of physiological large-scale networks such as correlated firing and inactive neurons. We tested connectivity derivation methods on ground-truth spiking data from detailed models of human cortical microcircuits in different layers and between key neuron types. We showed that physiological oscillations in the large-scale microcircuits hindered derivation accuracy, which was improved using a shorter cross-correlogram analysis window. We then showed that connection derivation was poor in cortical layer 2/3 microcircuits compared to layer 5, due to low firing rates and inactive neurons. General stimulation strategies for layer 2/3 microcircuits led to only a moderate improvement in derivation performance, due to a trade-off between the proportions of inactive neurons and overactive neurons, indicating the need for more refined strategies. Lastly, we showed that derivation of inhibitory connections from somatostatin interneurons targeting distal dendrites required a longer timescale of cross-correlation lags. Our results identify key physiological challenges and methods to improve accuracy in deriving connections from spiking activity in large-scale neuronal microcircuits.

Introduction

Information processing in the brain is governed by the activity of diverse neuron types[1–3] with specific connectivity[4–7]. Accordingly, cortical dysfunction has been associated with changes in microcircuit connectivity[8–11]. Accurately inferring the underlying cortical microcircuit connectivity is therefore essential for uncovering how information is processed in the brain in health and disease. Short-lag correlations from pairwise extracellular spiking have been commonly used to derive monosynaptic connectivity *in vivo*[12–14], and using these methods with high-density Neuropixels probes[15,16] can enable derivation of larger scale connectivity. However, studies have yet to address key physiological confounds of large-scale derivation such as inactive neurons[17] and correlated network firing[18].

There are several common methods for deriving connections, each with its advantages and limitations. Intracellular paired-recordings of postsynaptic potentials (PSP) enable direct detection and measuring of synaptic connection strength[19], but are limited in scale to at most a dozen neurons simultaneously[5]. Recent advancements allow for the switching the neurons being recorded, to yield tens of neurons from a single microcircuit[20]. Conversely, volume electron microscopy[21,22] offers a means for larger-scale connectome reconstruction of segments as large as 1 mm^3 [23–25], but these structural methods are limited in their ability to quantify synaptic connection strength[26,27]. Short-lags in spike cross-correlations between pairs of neurons in extracellular spike recordings[12,13] enable deriving putative monosynaptic connections and strengths[28,29] *in vivo*, and recent high-density Neuropixels probes[15] that record spiking in hundreds of neurons simultaneously[16,30] offer the advantage of estimating connections at large-scale.

Physiological confounds need to be considered when deriving connectivity in realistic large-scale networks. Correlated activity of neuronal microcircuits due to oscillations[18] or shared inputs[31,32] can lead to spurious derived connections. Inactive or silent neurons, for which spiking information is lacking, often constitute a significant portion of the neurons in the network, up to 30% in L2/3[17,33–35], and can lead to missed connections. Other physiological properties such as detailed neuron morphologies, multiple synaptic contacts, and stochastic release probabilities, all contribute to more complex relationship between synaptic inputs and spike output[36], which may impose challenges in connection derivation from cross-correlations.

Previous efforts have taken different approaches to improve neuronal connectivity derivation. Generalized linear models fit to cross-correlograms were used to improve the derivation accuracy and to estimate synaptic weights corresponding to PSPs[37,38]. Supervised

learning algorithms have been used to infer synaptic weights from presynaptic spike trains of simulated networks[39], and with perturbation strategies to address silent neurons[40]. Other studies developed methods to derive network connectivity from multiple samples via statistical connectivity inferencing[41,42]. However, all these previous studies used simplified small network models that did not address challenges of large-scale physiological microcircuits such as silent neurons and correlated activity due to circuit dynamics.

Here we test methods for deriving connections from cross-correlations using ground-truth spiking data from recent detailed large-scale models of human cortical microcircuits[43,44], accounting for several key physiological challenges. We characterize the effects of network oscillations in different layers, low firing rates and inactive neurons in L2/3, and we test general stimulation strategies to improve connection derivation. In addition to excitatory connections, we also examine derivation for different inhibitory connection types in the cortical microcircuits.

Results

We examined the performance of deriving putative monosynaptic connections from spike cross-correlations during baseline activity using ground-truth simulated data from our previous detailed models of human L5 microcircuits (Figure 1A). We used recent tools of fitting generalized linear models to cross-correlograms, featuring a slow fluctuation curve to absorb correlation trends in baseline activity over longer time courses.

When deriving excitatory connections across pyramidal (Pyr) neurons (n = 700) using long cross-correlogram windows such as ± 50 ms or ± 200 ms, sensitivity and specificity were good (sensitivity = 83.0 ± 5.7%; specificity = 96.0 ± 1.2%) but oscillation confounds led to high false positive rates and thus low PPV (67.3 ± 6.8%; Figure 1B-C). Different parameter values of the slow fluctuation curve, including using a wave period that matched the baseline cross-correlation fluctuations in the analysis window, did not improve the derivation performance. Instead, we found that shortening the analysis window relative to the oscillation period, e.g. to ± 20 ms, improved derivation performance by decreasing false positives and false negatives, thus improving PPV (84.5 ± 6.6%, Cohen's $d = 2.57$, $p < 0.05$) and sensitivity (88.2 ± 7.5%, Cohen's $d = 0.79$, $p < 0.05$), respectively (Figure 1C). There was a steady improvement in derivation performance with the length of simulated data up to 120 minutes (30 min vs 120 min: sensitivity = 49.0 ± 21.2% vs 85.2 ± 10.9%, Cohen's $d = 2.15$, $p < 0.05$,

Figure 1D), beyond which the improvement was only marginal (120 min vs 180 min: sensitivity = 85.2 ± 10.9% vs 88.2 ± 7.5%, Cohen's $d = 0.32$, $p < 0.05$, Figure 1D).

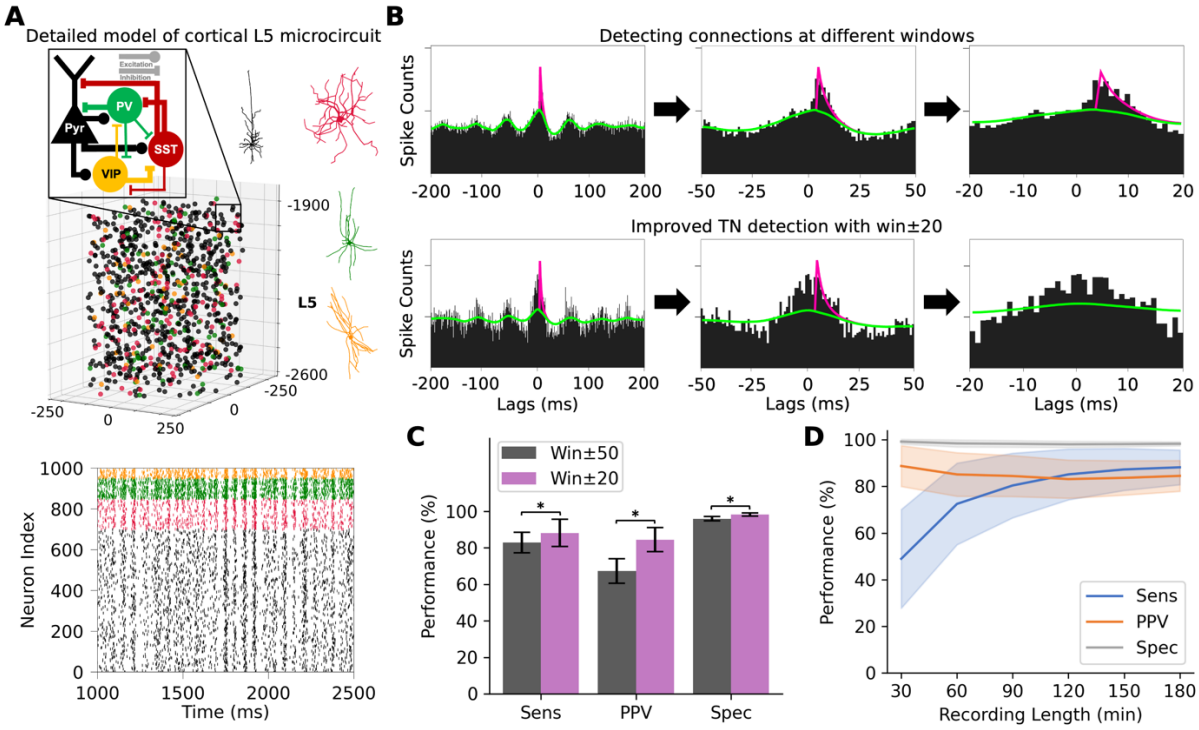

Figure 1. Overcoming the effects of oscillations on deriving excitatory connections in L5 microcircuits. (A) Top: The detailed model of human cortical L5 microcircuit comprised of 1,000 neurons of the key types (Pyr, SST, PV and VIP) with detail morphologies, distributed in a 500 x 500 x 700 μm^3 volume. Inset: schematic diagram of the excitatory and inhibitory connections between neuron types. Bottom: Example raster plot of baseline neuronal spiking used for connection derivation, color-coded according to neuron type. **(B)** Top: cross-correlogram, derived connection (magenta) and slow fluctuations curve (green) for an example true positive connection between two Pyr neurons, using ± 200 ms (left), ± 50 ms (middle), or ± 20 ms window (right). Bottom: Example false positive derivation at ± 200 ms (left) and ± 50 ms (middle) windows, which was correctly identified as a true negative using the ± 20 ms window (right). **(C)** Derivation performance for L5 excitatory connections using ± 50 ms (black) or ± 20 ms (purple) windows (n = 700 postsynaptic Pyr neurons). Asterisk denotes $p < 0.05$. **(D)** Derivation performance as a function of the length of simulated spike data in L5, using ± 20 ms window. Plots in C and D show mean ± SD.

We evaluated how the derivation methods perform for less active microcircuits, using simulated spiking data from our detailed models of human L2/3 cortical microcircuits. Baseline L2/3 Pyr neurons had a lower mean firing rate compared to L5 neurons (0.8 ± 0.6 Hz vs 3.3 ± 1.0 Hz, Cohen's $d = 2.97$, $p < 0.05$; Figure 2A). Consequently, derivation performance for L2/3 excitatory connections was poor (sensitivity = 5.6 ± 6.3%, n = 784 postsynaptic neurons; Figure 2B). As the cross-correlograms did not exhibit strong oscillations, it is likely that the higher proportion of false negatives was due to a lack of spike data from the low firing L2/3 Pyr neurons (Figure 2C).

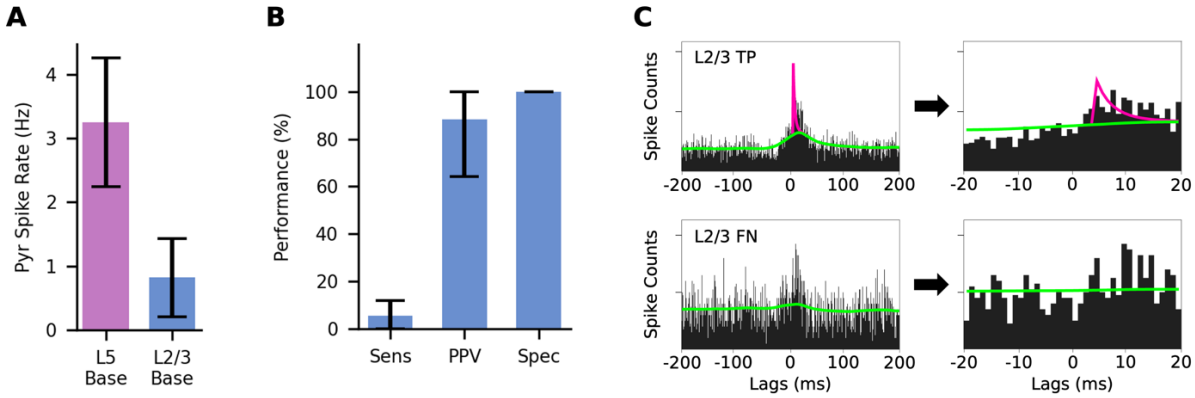

Figure 2. Low activity in L2/3 hinders derivation of excitatory connections. (A) Baseline Pyr neuron spike rate in L5 microcircuits (purple, n = 700 neurons) and L2/3 microcircuits (blue, n = 784 neurons). **(B)** Derivation performance for Pyr neurons in L2/3 microcircuit at baseline. **(C)** Cross-correlogram, derived connection (magenta) and slow fluctuations curve (green) for example true positive (top) and example false negative (bottom) derivation of excitatory connections in the L2/3 microcircuit, using ± 200 ms and ± 20 ms windows. Histograms in A and B show mean ± SD.

We therefore tested a general activation of L2/3 Pyr neurons by increasing their background input, thus increasing the mean firing rate to 3.3 ± 2.4 Hz, close to that in L5 (Figure 3A). Derivation performance for the activated L2/3 had higher sensitivity (52.7 ± 14.0%, Cohen's $d = 4.34$, $p < 0.05$, n = 786 neurons; Figure 3B), although still low compared to the L5 case. While the activation decreased PPV to some extent (L2/3 baseline: PPV = 88.4 ± 24.2%, n = 784 neurons; L2/3 activated: PPV = 69.9 ± 13.7%, Cohen's $d = -0.94$, $p < 0.05$, n = 786 neurons; Figure 3B), the increase in sensitivity was much larger, therefore the derivation performance was overall better and more balanced than at baseline.

A likely reason for the moderate improvement by activating L2/3 using a general stimulation of Pyr neurons is indicated by the distribution of average Pyr neuron spike rates (Figure 3A). While the activated L2/3 Pyr neurons had much less inactive neurons compared to baseline L2/3, there were still 17% (n = 133) inactive neurons firing at < 1 Hz, and the sensitivity in deriving connections for these neurons was poorer than average (12.4 ± 10.9%, Cohen's $d = -2.97$, $p < 0.05$). There was also a larger right tail compared to L5, with a considerable proportion (25%, n = 200) overactive neurons firing at > 5 Hz, for which the sensitivity in connection derivation was poorer than average too (14.1 ± 8.0%, Cohen's $d = -2.98$, $p < 0.05$). The main reason for the low sensitivity in the case of overactive neurons is a large proportion of false negatives that were estimated as non-connections due to peaks at lag 0 ms in the cross-correlograms, resulting from higher spike correlations between the overactive neurons than average (0.008 ± 0.0001 vs 0.005 ± 0.00008, Cohen's $d > 3$, $p < 0.05$). A reason for the lower PPV performance was that the increased firing of the overactive neurons resulted

from recurrent activity, and thus followed underactive neurons, leading to short-lag peaks in the cross-correlograms irrespective of connectivity and thus spurious connection derivation. In comparison, the remaining 58% (n = 453) of the neurons, which fired between 1 – 5 Hz, showed better connection derivation compared to average performance (sensitivity 70.0 ± 9.1%, Cohen's $d = 1.4$, $p < 0.05$).

We therefore tested another general stimulation strategy that yielded a distribution of average L2/3 Pyr neuron spiking similar to L5 in addition to a similar mean Pyr firing rate of 3.4 ± 1.3 Hz. This strategy involved a disinhibition of Pyr neurons by decreasing background input to PV and SST interneurons, together with a small decrease in Pyr background inputs. However, this stimulation by disinhibition led to more rhythmic and correlated firing than baseline (0.07 ± 0.001 vs 0.0008 ± 0.00002 vs, Cohen's $d > 3$, $p < 0.05$ Figure 3C), which resulted in increased spurious (false positive) derivation and thus poor PPV compared to baseline (29.1 ± 9.8%, Cohen's $d = -3.23$, $p < 0.05$, n = 800 neurons; Figure 3B). The disinhibition led to only a modest increase in sensitivity compared to baseline (34.3 ± 17.3%, Cohen's $d = 2.19$, $p < 0.05$, n = 800 neurons; Figure 3B) and thus was overall less successful than the activation strategy.

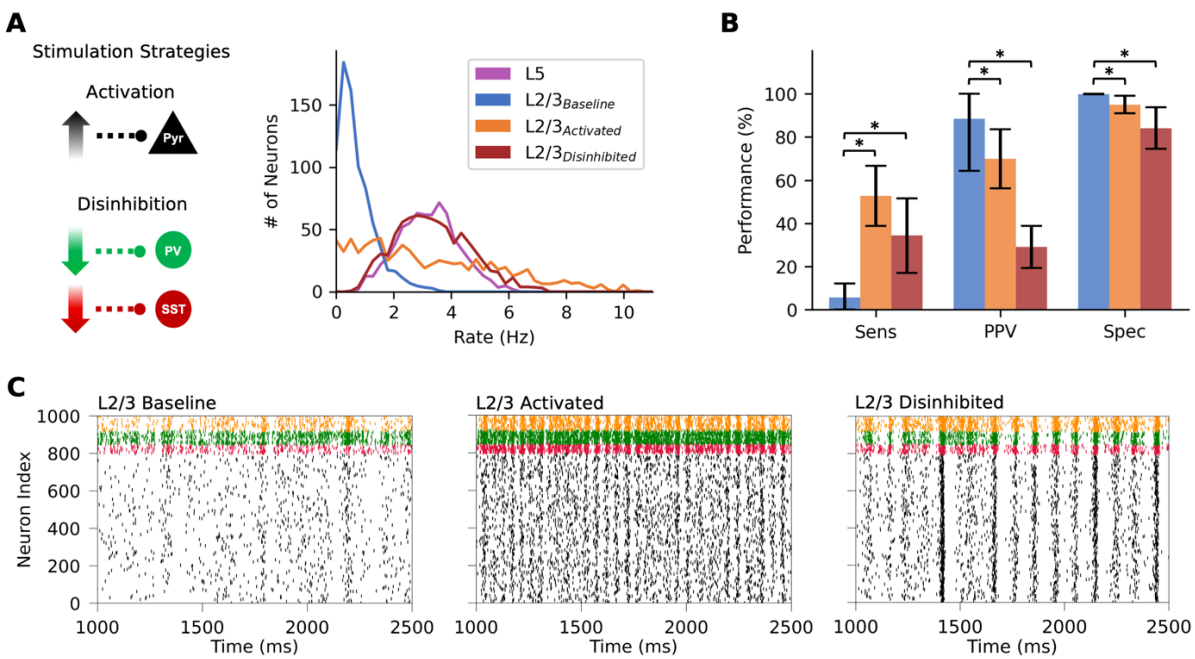

Figure 3. Moderate improvement in derivation of L2/3 connections by general stimulation of Pyr neurons. (A) Left: The strategies for general stimulation of Pyr neurons in the microcircuit, either activating or disinhibiting Pyr neurons. Right: Distribution of Pyr neuron spike rates in L5 baseline (purple, n = 700), L2/3 baseline (blue, n = 784), L2/3 activated (orange, n = 786), and L2/3 disinhibited (red, n = 800). **(B)** Derivation performance (mean ± SD) for excitatory connections in L2/3 microcircuits at baseline, activated and disinhibited conditions (color-coded as in A). Asterisk denotes $p < 0.05$. **(C)** Example raster plot of simulated spiking in L2/3 microcircuits at baseline (left), activated (middle), and disinhibited (right) conditions, color-coded according to neuron type.

We next compared derivation for connections from different inhibitory interneuron types onto Pyr neurons. Whereas PV→Pyr connections targeted proximal regions of the Pyr neuron (basal dendrites and soma), and could be derived using a short time scale like the Pyr→Pyr connections ($\tau = 4$ ms in both layers 2/3 and 5, Figure 4A), SST interneurons targeted distal regions (apical dendrites) and thus required using a longer decay time constant ($\tau = 8$ ms and $\tau = 15$ ms for SST→Pyr in L5 and L2/3, respectively, Figure 4B).

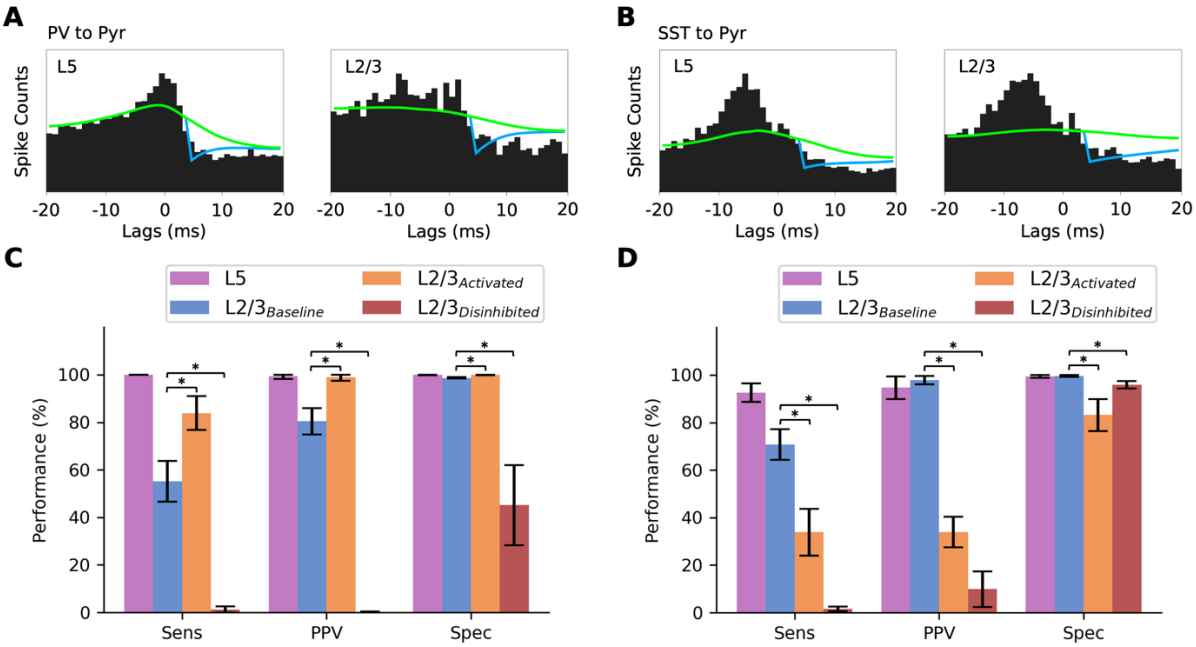

Figure 4. Connection derivation for PV vs SST inhibitory connections. (A) Cross-correlogram, derived connection (cyan) and slow fluctuation curve (green) for example derivations of true positive PV→Pyr connections in L5 (left) and L2/3 (right) microcircuits. **(B)** Same as A, but for SST→Pyr connections. **(C)** Derivation performance for PV→Pyr inhibitory connections in the different conditions. **(D)** Same as C, but for SST→Pyr connections. Asterisk denotes $p < 0.05$. Histograms in C and D show mean ± SD.

For the L5 microcircuit, inhibitory connections were detected with high accuracy for both PV→Pyr (sensitivity = 100.0 ± 0.0%; PPV = 99.4 ± 1.2%; n = 100 presynaptic neurons; Figure 4C) and SST→Pyr (sensitivity = 92.5 ± 3.9%; PPV = 94.7 ± 4.8%; n = 150 presynaptic neurons; Figure 4D). In the L2/3 microcircuit at baseline, however, detection accuracy was lower for both PV→Pyr connections (sensitivity = 55.1 ± 8.6%; PPV = 80.4 ± 5.6%; n = 70 presynaptic neurons; Figure 4C) and SST→Pyr connections (sensitivity = 70.8 ± 6.5%; PPV = 97.8 ± 1.8%; n = 50 presynaptic neurons; Figure 4D), although better than for Pyr→Pyr connections. Derivation performance for these connections was averaged across presynaptic interneurons instead of postsynaptic pyramidal neurons to ensure adequate sample sizes. The low sensitivity in L2/3 at baseline was likely mostly due to the low firing rates in Pyr neurons, as SST and PV interneurons fired at moderate rates (5.7 ± 0.9 Hz and 10.2 ± 2.9 Hz,

respectively). The higher accuracy in SST→Pyr derivation compared to PV→Pyr in L2/3 baseline was likely due to the use of a longer decay time constant and thus larger information about the effects on postsynaptic neuron spiking in cross-correlations.

Activating L2/3 microcircuits by general stimulation of Pyr neurons improved detection performance in PV→Pyr connections (sensitivity = 83.9 ± 7.1%, Cohen's $d = 3.63$, $p < 0.05$; PPV = 99.1 ± 1.6%, Cohen's $d = 4.50$, $p < 0.05$; Figure 4C), due to increased postsynaptic Pyr firing rates. The sensitivity was still lower than in L5 derivation, likely due to issues with the inactive and overactive postsynaptic Pyr neurons described above for Pyr→Pyr connection derivation. Derivation accuracy for SST→Pyr connections decreased considerably in the activated L2/3 microcircuit instead of improving (sensitivity = 33.9 ± 9.8%, Cohen's $d = -4.40$, $p < 0.05$; PPV = 33.9 ± 6.5%, Cohen's $d = -13.33$, $p < 0.05$, Figure 4D). This was due to the drastic increase in SST firing rates in the activated L2/3 microcircuit (24.5 ± 5.4 Hz) and higher correlated firing of SST and Pyr neurons (SST-Pyr: 0.02 ± 0.0002 vs 0.002 ± 0.00005, Cohen's $d > 3$, $p < 0.05$; SST-SST: 0.06 ± 0.0006 vs 0.009 ± 0.0002, Cohen's $d > 3$, $p < 0.05$), leading to spurious connection derivation (false positives) and ignored connections (false negatives) due to lag 0 peaks in the cross-correlogram. Disinhibiting the L2/3 microcircuit resulted in even poorer derivation performance for both types of connections (PV→Pyr: sensitivity = 1.3 ± 1.3%, Cohen's $d = -8.70$, $p < 0.05$, Figure 4C; SST→Pyr: sensitivity = 1.6 ± 1.0%, Cohen's $d = -14.71$, $p < 0.05$, Figure 4D), due to even higher correlated firing in the microcircuit (SST-SST: 0.2 ± 0.001, Cohen's $d > 3$, $p < 0.05$; PV-PV: 0.2 ± 0.0001, Cohen's $d > 3$, $p < 0.05$; PV-Pyr: 0.1 ± 0.001, Cohen's $d > 3$, $p < 0.05$).

Derivation accuracy for connections between different inhibitory interneurons was moderate for PV→SST and VIP→SST connections in L5 microcircuits (sensitivity for PV→SST: 57.9 ± 16.5%; VIP→SST: 68.8 ± 15.0%) and in L2/3 microcircuits at baseline (sensitivity for PV→SST: 70.6 ± 33.1%; VIP→SST: 52.6 ± 12.6%), but poor for the rest of the connections between inhibitory interneurons. For similar reasons as described above, activating or disinhibiting L2/3 Pyr neurons did not improve the performance for these connections either.

Discussion

In this work, we examined physiological challenges of deriving neuronal connectivity from baseline spiking activity, using detailed models of large-scale human cortical microcircuits in different layers. We showed that physiological properties of large-scale

microcircuits had a significant impact on the accuracy of deriving Pyr neuron connections from spiking cross-correlograms. Correlated activity due to oscillations led to considerable false positives and required using a short analysis window, whereas silent neurons in certain cortical layers posed a limit to derivation accuracy in terms of false negatives. We further showed that a general activation of cortical microcircuits to increase firing rates yielded only a moderate improvement in connection derivation due to a trade-off between low and high firing neurons, indicating that more refined activations are needed. We compared derivation for different inhibitory connection types and found that SST interneuron connections required a longer range of cross-correlation lags compared to PV interneurons, due to their distal synaptic contacts. Our results addressing physiological challenges of correlated microcircuit activity, low/silent firing, and different connection types can serve to inform experimental efforts to improve connection derivation accuracy.

Connection derivation in our microcircuit models required a slightly longer synaptic delay compared to previous studies[13,37]. A possible reason is that traditional parameters were based on rodent data, where neurons have shorter and less complex dendritic arbors than human neurons[45–47], and thus the delay between presynaptic spike and PSP at soma is shorter. While the cross-correlogram lag range used for connection derivation was comparable to previous studies, good derivation of L2/3 SST→Pyr connections necessitated a longer lag range compared to PV→Pyr connections due to the attenuation of SST IPSP from the distal apical synapses to the soma[48,49]. Deriving L5 SST→Pyr connections also required a long range but to a lesser extent, since human L5 Pyr neuron apical dendrites were less branched than those of L2/3 Pyr neurons in the reconstructed morphologies we used, and also on average as reported previously[43,44]. The proximal locations of PV→Pyr synapses resulted in stronger connections compared to SST→Pyr, explaining the overall better derivation performance in L5, and a better improvement when activating L2/3. In this work we focused on connection detection rather than weight derivation, since the microcircuit models had the same conductance for all connections of a given type, with only the contact locations varying, resulting in a low range of synaptic weights. Future models should account for wider synaptic weight distributions as seen in the cortex[4] to study derivation performance in terms of connection weight.

Overcoming the challenge of microcircuit oscillations required shortening the cross-correlogram analysis window to less than the oscillation period, as it enabled the slow wave of the tool to better fit the baseline fluctuations near lag 0 and thus better detect connections on top of the baseline cross-correlation. However, the tool's components were not sufficient to fit the overall shape of the cross-correlogram trough of inhibitory SST→Pyr connections which

involved a slower rise time, resulting in moderate derivation accuracy and highlighting the tool's limitation of having only one time constant parameter. Future studies should try to improve the tool by including both rise and decay time constants in the coupling filter.

The L2/3 microcircuit stimulation strategies aimed to increase the average firing rate of Pyr neurons to resemble L5, which was active enough to yield good derivation. However, unlike the normal distribution of moderate firing rates in L5, the L2/3 activated Pyr neurons had populations of overactive and remaining underactive neurons hindering derivation performance. These results suggest that general stimulation, e.g. by pharmacology applied to the entire circuit[50], may have limited use with regards to connection derivation. More complex perturbation protocols could include modeling a variety of sensory stimulus presentations e.g. using different orientations[44,51] or motion tasks[52,53] to activate different subgroups of neurons at a time.

Future works can refine our estimates of derivation accuracy by addressing issues that would arise from extracellular recordings such as noise[18,54] and spike sorting[55–57]. In addition, including a larger portion of silent neurons as suggested experimentally[17,33–35] and shared inputs among the neurons in the microcircuits[31,32] will help refine the estimated accuracy and the necessary stimulation strategies. Future studies can also probe the effects of morphology[36] or physiological synaptic features such as multiple contacts, failure probability[58,59] and short-term dynamics on connection derivation.

Methods

Human cortical microcircuit models: We used detailed models of human cortical L5 microcircuits[44] and L2/3 microcircuits[43] as ground-truth data. Both microcircuit models consisted of 1000 detailed neuron models that reproduced firing rates, synaptic properties, and dendritic sag currents as measured in human neurons. Pyr→Pyr connection probability was 0.15 for L2/3 and 0.09 for L5, as measured in humans, and other connection probabilities were as measured in rodents. The neurons were radially distributed in a volume with a 250 μm radius and a depth according to human cortical layer dimensions[60]. The models included key neuron types and proportions measured in humans; L5 circuit: 70% pyramidal neurons (Pyr), 15% somatostatin-expressing interneurons (SST), 10% parvalbumin-expressing interneurons (PV), and 5% vasoactive intestinal peptide-expressing interneurons (VIP)[44]. L2/3 circuit: 80% Pyr, 5% SST, 7% PV, 8% VIP[43]. The microcircuit models received random background excitatory inputs (neuron type specific) using Ornstein-Uhlenbeck (OU) point processes[61,62].

Neuronal connectivity derivation: We inferred putative monosynaptic connections by detecting short-lag peaks in cross-correlograms of simulated spike trains[13,37]. We used previous GLM methods for fitting postsynaptic waveform curves to cross-correlograms[37] for improved derivation. We did a parameter search for the synaptic delay (d_s), interaction timescale (τ), and flatness of slow fluctuation curve (γ) that yielded the best derivation performance. We tested synaptic delays ranging from d_s = 1 to 4 ms and slow fluctuation curves ranging from $\gamma = 2 \times 10^{-4}$ ms^{-1} (flatter) to 1×10^{-3} ms^{-1} (oscillatory). We determined the combination of d_s = 4 ms and $\gamma = 2 \times 10^{-4}$ ms^{-1} led to more balanced connection derivation performance. We used τ = 4 ms for all connection types except SST→Pyr (L5: τ = 8 ms, L2/3: τ = 15 ms), which required a longer τ due to the distal location of the synapses.

When deriving connections, we excluded silent neurons firing < 0.1 Hz as the lack of spike data incurred an error in the GLM tool and was not amenable to cross-correlation analysis. We evaluated derivation performance by calculating the sensitivity, positive predictive value (PPV), and specificity.

Neuronal stimulation: We tested two general stimulations of L2/3 Pyr neurons to increase microcircuit activity, by changing background inputs to specific neuron types. L2/3 baseline excitatory OU conductance was: Pyr = 28 pS; SST = 30 pS; PV = 280 pS; VIP = 66 pS. In the L2/3 activated case, background OU conductance in Pyr neurons was increased to 50 pS. In the L2/3 disinhibited case, background OU conductance in SST and PV interneurons was reduced to 28 and 1 pS, respectively, and slightly reduced in Pyr neurons to 24 pS. Other disinhibition strategies were less useful, e.g. reducing SST alone attenuated the overactive population at the expense of an increased proportion of low firing Pyr neuron population, and reducing PV alone led to a broad distribution with highly correlated firing. A combination of both was thus necessary to achieve the desired mean and distribution. In all cases, the inhibitory component of the OU conductance was set to 0, as the recurrent inhibition in the microcircuit was sufficient to restrain excitability.

Correlation tests: Discrete cross-correlations between neuron spike trains were calculated using normalized signals of spike time vectors with 3 ms bins. Before correlating, spike time vectors were normalized by subtracting the mean from the signals and dividing by the product of the standard deviation and the vector length[63–65].

Statistical analysis: We determined statistical significance ($p < 0.05$) using paired and two-sample t-tests. We calculated the effect size between two conditions using Cohen's *d* (dividing the difference of two means by the overall standard deviation of all values).

References

1. Gentet, L. J., Kremer, Y., Taniguchi, H., Huang, Z. J., Staiger, J. F., & Petersen, C. C. H. (2012). Unique functional properties of somatostatin-expressing GABAergic neurons in mouse barrel cortex. *Nature Neuroscience*, *15*(4), 607–612. https://doi.org/10.1038/nn.3051

2. Gal, E., London, M., Globerson, A., Ramaswamy, S., Reimann, M. W., Muller, E., Markram, H., & Segev, I. (2017). Rich cell-type-specific network topology in neocortical microcircuitry. *Nature Neuroscience*, *20*(7), 1004–1013. https://doi.org/10.1038/nn.4576

3. Yu, J., Hu, H., Agmon, A., & Svoboda, K. (2019). Recruitment of GABAergic Interneurons in the Barrel Cortex during Active Tactile Behavior. *Neuron*, *104*(2), 412-427.e4. https://doi.org/10.1016/j.neuron.2019.07.027

4. Song, S., Sjöström, P. J., Reigl, M., Nelson, S., & Chklovskii, D. B. (2005). Highly Nonrandom Features of Synaptic Connectivity in Local Cortical Circuits. *PLOS Biology*, *3*(3), e68. https://doi.org/10.1371/journal.pbio.0030068

5. Perin, R., Berger, T. K., & Markram, H. (2011). A synaptic organizing principle for cortical neuronal groups. *Proceedings of the National Academy of Sciences*, *108*(13), 5419–5424. https://doi.org/10.1073/pnas.1016051108

6. Campagnola, L., Seeman, S. C., Chartrand, T., Kim, L., Hoggarth, A., Gamlin, C., Ito, S., Trinh, J., Davoudian, P., Radaelli, C., Kim, M.-H., Hage, T., Braun, T., Alfiler, L., Andrade, J., Bohn, P., Dalley, R., Henry, A., Kebede, S., … Jarsky, T. (2022). Local connectivity and synaptic dynamics in mouse and human neocortex. *Science*, *375*(6585), eabj5861. https://doi.org/10.1126/science.abj5861

7. Sharf, T., van der Molen, T., Glasauer, S. M. K., Guzman, E., Buccino, A. P., Luna, G., Cheng, Z., Audouard, M., Ranasinghe, K. G., Kudo, K., Nagarajan, S. S., Tovar, K. R., Petzold, L. R., Hierlemann, A., Hansma, P. K., & Kosik, K. S. (2022). Functional neuronal circuitry and oscillatory dynamics in human brain organoids. *Nature Communications*, *13*(1), 4403. https://doi.org/10.1038/s41467-022-32115-4

8. Seney, M. L., Tripp, A., McCune, S., A. Lewis, D., & Sibille, E. (2015). Laminar and cellular analyses of reduced somatostatin gene expression in the subgenual anterior cingulate cortex in major depression. *Neurobiology of Disease*, *73*, 213–219. https://doi.org/10.1016/j.nbd.2014.10.005

9. Duman, R. S., Sanacora, G., & Krystal, J. H. (2019). Altered Connectivity in Depression: GABA and Glutamate Neurotransmitter Deficits and Reversal by Novel Treatments. *Neuron*, *102*(1), 75–90. https://doi.org/10.1016/j.neuron.2019.03.013

10. Lazarus, M. S., Krishnan, K., & Huang, Z. J. (2015). GAD67 Deficiency in Parvalbumin Interneurons Produces Deficits in Inhibitory Transmission and Network Disinhibition in Mouse Prefrontal Cortex. *Cerebral Cortex (New York, NY)*, *25*(5), 1290–1296. https://doi.org/10.1093/cercor/bht322

11. Toker, L., Mancarci, B. O., Tripathy, S., & Pavlidis, P. (2018). Transcriptomic Evidence for Alterations in Astrocytes and Parvalbumin Interneurons in Subjects With Bipolar Disorder and Schizophrenia. *Biological Psychiatry*, *84*(11), 787–796. https://doi.org/10.1016/j.biopsych.2018.07.010

12. Barthó, P., Hirase, H., Monconduit, L., Zugaro, M., Harris, K. D., & Buzsáki, G. (2004). Characterization of Neocortical Principal Cells and Interneurons by Network Interactions and Extracellular Features. *Journal of Neurophysiology*, *92*(1), 600–608. https://doi.org/10.1152/jn.01170.2003

13. Peyrache, A., Dehghani, N., Eskandar, E. N., Madsen, J. R., Anderson, W. S., Donoghue, J. A., Hochberg, L. R., Halgren, E., Cash, S. S., & Destexhe, A. (2012). Spatiotemporal dynamics of neocortical excitation and inhibition during human sleep. *Proceedings of the National Academy of Sciences*, *109*(5), 1731–1736. https://doi.org/10.1073/pnas.1109895109

14. Vizuete, J. A., Pillay, S., Diba, K., Ropella, K. M., & Hudetz, A. G. (2012). Monosynaptic functional connectivity in cerebral cortex during wakefulness and under graded levels of anesthesia. *Frontiers in Integrative Neuroscience*, *6*, 90. https://doi.org/10.3389/fnint.2012.00090

15. Jun, J. J., Steinmetz, N. A., Siegle, J. H., Denman, D. J., Bauza, M., Barbarits, B., Lee, A. K., Anastassiou, C. A., Andrei, A., Aydın, Ç., Barbic, M., Blanche, T. J., Bonin, V., Couto, J., Dutta, B., Gratiy, S. L., Gutnisky, D. A., Häusser, M., Karsh, B., … Harris, T. D. (2017). Fully integrated silicon probes for high-density recording of neural activity. *Nature*, *551*(7679), 232–236. https://doi.org/10.1038/nature24636

16. Steinmetz, N. A., Aydin, C., Lebedeva, A., Okun, M., Pachitariu, M., Bauza, M., Beau, M., Bhagat, J., Böhm, C., Broux, M., Chen, S., Colonell, J., Gardner, R. J., Karsh, B., Kloosterman, F., Kostadinov, D., Mora-Lopez, C., O'Callaghan, J., Park, J., … Harris, T. D. (2021). Neuropixels 2.0: A miniaturized high-density probe for stable, long-term brain recordings. *Science*, *372*(6539), eabf4588. https://doi.org/10.1126/science.abf4588

17. Shoham, S., O'Connor, D. H., & Segev, R. (2006). How silent is the brain: Is there a "dark matter" problem in neuroscience? *Journal of Comparative Physiology A*, *192*(8), 777–784. https://doi.org/10.1007/s00359-006-0117-6

18. Buzsáki, G., & Draguhn, A. (2004). Neuronal Oscillations in Cortical Networks. *Science*, *304*(5679), 1926–1929. https://doi.org/10.1126/science.1099745

19. Noguchi, A., Ikegaya, Y., & Matsumoto, N. (2021). In Vivo Whole-Cell Patch-Clamp Methods: Recent Technical Progress and Future Perspectives. *Sensors (Basel, Switzerland)*, *21*(4), 1448. https://doi.org/10.3390/s21041448

20. Peng, Y., Mittermaier, F. X., Planert, H., Schneider, U. C., Alle, H., & Geiger, J. R. P. (2019). High-throughput microcircuit analysis of individual human brains through next-generation multineuron patch-clamp. *eLife*, *8*, e48178. https://doi.org/10.7554/eLife.48178

21. Kubota, Y., Sohn, J., & Kawaguchi, Y. (2018). Large Volume Electron Microscopy and Neural Microcircuit Analysis. *Frontiers in Neural Circuits*, *12*. https://www.frontiersin.org/articles/10.3389/fncir.2018.00098

22. Peddie, C. J., Genoud, C., Kreshuk, A., Meechan, K., Micheva, K. D., Narayan, K., Pape, C., Parton, R. G., Schieber, N. L., Schwab, Y., Titze, B., Verkade, P., Weigel, A., & Collinson, L. M. (2022). Volume electron microscopy. *Nature Reviews Methods Primers*, *2*(1), Article 1. https://doi.org/10.1038/s43586-022-00131-9

23. Hayworth, K. J., Xu, C. S., Lu, Z., Knott, G. W., Fetter, R. D., Tapia, J. C., Lichtman, J. W., & Hess, H. F. (2015). Ultrastructurally smooth thick partitioning and volume stitching for large-scale connectomics. *Nature Methods*, *12*(4), 319–322. https://doi.org/10.1038/nmeth.3292

24. Zheng, Z., Lauritzen, J. S., Perlman, E., Robinson, C. G., Nichols, M., Milkie, D., Torrens, O., Price, J., Fisher, C. B., Sharifi, N., Calle-Schuler, S. A., Kmecova, L., Ali, I. J., Karsh, B., Trautman, E. T., Bogovic, J. A., Hanslovsky, P., Jefferis, G. S. X. E., Kazhdan, M., … Bock, D. D. (2018). A Complete Electron Microscopy Volume of the Brain of Adult Drosophila melanogaster. *Cell*, *174*(3), 730-743.e22. https://doi.org/10.1016/j.cell.2018.06.019

25. Shapson-Coe, A., Januszewski, M., Berger, D. R., Pope, A., Wu, Y., Blakely, T., Schalek, R. L., Li, P. H., Wang, S., Maitin-Shepard, J., Karlupia, N., Dorkenwald, S., Sjostedt, E., Leavitt, L., Lee, D., Troidl, J., Collman, F., Bailey, L., Fitzmaurice, A., … Lichtman, J. W. (2024). A petavoxel fragment of human cerebral cortex reconstructed at nanoscale resolution. *Science*, *384*(6696), eadk4858. https://doi.org/10.1126/science.adk4858

26. Schneider-Mizell, C. M., Gerhard, S., Longair, M., Kazimiers, T., Li, F., Zwart, M. F., Champion, A., Midgley, F. M., Fetter, R. D., Saalfeld, S., & Cardona, A. (2016). Quantitative neuroanatomy for connectomics in Drosophila. *eLife*, *5*, e12059. https://doi.org/10.7554/eLife.12059

27. Dorkenwald, S., Schubert, P. J., Killinger, M. F., Urban, G., Mikula, S., Svara, F., & Kornfeld, J. (2017). Automated synaptic connectivity inference for volume electron microscopy. *Nature Methods*, *14*(4), Article 4. https://doi.org/10.1038/nmeth.4206

28. Fujisawa, S., Amarasingham, A., Harrison, M. T., & Buzsáki, G. (2008). Behavior-dependent short-term assembly dynamics in the medial prefrontal cortex. *Nature Neuroscience*, *11*(7), 823–833. https://doi.org/10.1038/nn.2134

29. De Blasi, S., Ciba, M., Bahmer, A., & Thielemann, C. (2019). Total spiking probability edges: A cross-correlation based method for effective connectivity estimation of cortical spiking neurons. *Journal of Neuroscience Methods*, *312*, 169–181. https://doi.org/10.1016/j.jneumeth.2018.11.013

30. Siegle, J. H., Jia, X., Durand, S., Gale, S., Bennett, C., Graddis, N., Heller, G., Ramirez, T. K., Choi, H., Luviano, J. A., Groblewski, P. A., Ahmed, R., Arkhipov, A., Bernard, A., Billeh, Y. N., Brown, D., Buice, M. A., Cain, N., Caldejon, S., … Koch, C. (2021). Survey of spiking in the mouse visual system reveals functional hierarchy. *Nature*, *592*(7852), 86–92. https://doi.org/10.1038/s41586-020-03171-x

31. Ecker, A. S., Berens, P., Keliris, G. A., Bethge, M., Logothetis, N. K., & Tolias, A. S. (2010). Decorrelated Neuronal Firing in Cortical Microcircuits. *Science*, *327*(5965), 584–587.

32. Renart, A., de la Rocha, J., Bartho, P., Hollender, L., Parga, N., Reyes, A., & Harris, K. D. (2010). The Asynchronous State in Cortical Circuits. *Science*, *327*(5965), 587–590.

33. Gur, M., Kagan, I., & Snodderly, D. M. (2005). Orientation and Direction Selectivity of Neurons in V1 of Alert Monkeys: Functional Relationships and Laminar Distributions. *Cerebral Cortex*, *15*(8), 1207–1221. https://doi.org/10.1093/cercor/bhi003

34. Gur, M., & Snodderly, D. M. (2008). Physiological differences between neurons in layer 2 and layer 3 of primary visual cortex (V1) of alert macaque monkeys. *The Journal of Physiology*, *586*(9), 2293–2306. https://doi.org/10.1113/jphysiol.2008.151795

35. O'Connor, D. H., Peron, S. P., Huber, D., & Svoboda, K. (2010). Neural Activity in Barrel Cortex Underlying Vibrissa-Based Object Localization in Mice. *Neuron*, *67*(6), 1048–1061. https://doi.org/10.1016/j.neuron.2010.08.026

36. Beniaguev, D., Segev, I., & London, M. (2021). Single cortical neurons as deep artificial neural networks. *Neuron*, *109*(17), 2727-2739.e3. https://doi.org/10.1016/j.neuron.2021.07.002

37. Kobayashi, R., Kurita, S., Kurth, A., Kitano, K., Mizuseki, K., Diesmann, M., Richmond, B. J., & Shinomoto, S. (2019). Reconstructing neuronal circuitry from parallel spike trains. *Nature Communications*, *10*(1), 4468. https://doi.org/10.1038/s41467-019-12225-2

38. Endo, D., Kobayashi, R., Bartolo, R., Averbeck, B. B., Sugase-Miyamoto, Y., Hayashi, K., Kawano, K., Richmond, B. J., & Shinomoto, S. (2021). A convolutional neural network for estimating synaptic connectivity from spike trains. *Scientific Reports*, *11*(1), 12087. https://doi.org/10.1038/s41598-021-91244-w

39. Vareberg, A. D., Bok, I., Eizadi, J., Ren, X., & Hai, A. (2024). Inference of network connectivity from temporally binned spike trains. *Journal of Neuroscience Methods*, *404*, 110073. https://doi.org/10.1016/j.jneumeth.2024.110073

40. Ren, X., Bok, I., Vareberg, A., & Hai, A. (2023). Stimulation-mediated reverse engineering of silent neural networks. *Journal of Neurophysiology*, *129*(6), 1505–1514. https://doi.org/10.1152/jn.00100.2023

41. Vidne, M., Ahmadian, Y., Shlens, J., Pillow, J. W., Kulkarni, J., Litke, A. M., Chichilnisky, E. J., Simoncelli, E., & Paninski, L. (2012). Modeling the impact of common noise inputs on the network activity of retinal ganglion cells. *Journal of Computational Neuroscience*, *33*(1), 97–121. https://doi.org/10.1007/s10827-011-0376-2

42. Soudry, D., Keshri, S., Stinson, P., Oh, M., Iyengar, G., & Paninski, L. (2015). Efficient 'Shotgun' Inference of Neural Connectivity from Highly Sub-sampled Activity Data. *PLOS Computational Biology*, *11*(10), e1004464. https://doi.org/10.1371/journal.pcbi.1004464

43. Yao, H. K., Guet-McCreight, A., Mazza, F., Chameh, H. M., Prevot, T. D., Griffiths, J. D., Tripathy, S. J., Valiante, T. A., Sibille, E., & Hay, E. (2022). Reduced inhibition in depression impairs stimulus processing in human cortical microcircuits. *Cell Reports*, *38*(2). https://doi.org/10.1016/j.celrep.2021.110232

44. Guet-McCreight, A., Chameh, H. M., Mahallati, S., Wishart, M., Tripathy, S. J., Valiante, T. A., & Hay, E. (2023). Age-dependent increased sag amplitude in human pyramidal neurons dampens baseline cortical activity. *Cerebral Cortex*, *33*(8), 4360–4373. https://doi.org/10.1093/cercor/bhac348

45. Mihaljević, B., Larrañaga, P., Benavides-Piccione, R., DeFelipe, J., & Bielza, C. (2020). Comparing basal dendrite branches in human and mouse hippocampal CA1 pyramidal neurons with Bayesian networks. *Scientific Reports*, *10*(1), 18592. https://doi.org/10.1038/s41598-020-73617-9

46. Kalmbach, B. E., Hodge, R. D., Jorstad, N. L., Owen, S., Frates, R. de, Yanny, A. M., Dalley, R., Mallory, M., Graybuck, L. T., Radaelli, C., Keene, C. D., Gwinn, R. P., Silbergeld, D. L., Cobbs, C., Ojemann, J. G., Ko, A. L., Patel, A. P., Ellenbogen, R. G., Bakken, T. E., … Ting, J. T. (2021). Signature morpho-electric, transcriptomic, and dendritic properties of human layer 5 neocortical pyramidal neurons. *Neuron*, *109*(18), 2914-2927.e5. https://doi.org/10.1016/j.neuron.2021.08.030

47. Moradi Chameh, H., Rich, S., Wang, L., Chen, F.-D., Zhang, L., Carlen, P. L., Tripathy, S. J., & Valiante, T. A. (2021). Diversity amongst human cortical pyramidal neurons revealed via their sag currents and frequency preferences. *Nature Communications*, *12*(1), 2497. https://doi.org/10.1038/s41467-021-22741-9

48. Kole, M. H. P., Letzkus, J. J., & Stuart, G. J. (2007). Axon Initial Segment Kv1 Channels Control Axonal Action Potential Waveform and Synaptic Efficacy. *Neuron*, *55*(4), 633–647. https://doi.org/10.1016/j.neuron.2007.07.031

49. Alberts, B., Johnson, A., Lewis, J., Raff, M., Roberts, K., & Walter, P. (2002). Ion Channels and the Electrical Properties of Membranes. In *Molecular Biology of the Cell. 4th edition*. Garland Science. https://www.ncbi.nlm.nih.gov/books/NBK26910/

50. Florez, C. M., McGinn, R. J., Lukankin, V., Marwa, I., Sugumar, S., Dian, J., Hazrati, L.-N., Carlen, P. L., Zhang, L., & Valiante, T. A. (2015). In Vitro Recordings of Human Neocortical Oscillations. *Cerebral Cortex*, *25*(3), 578–597. https://doi.org/10.1093/cercor/bht235

51. Song, W., & Semework, M. (2015). Tactile representation in somatosensory thalamus (VPL) and cortex (S1) of awake primate and the plasticity induced by VPL neuroprosthetic stimulation. *Brain Research*, *1625*, 301–313. https://doi.org/10.1016/j.brainres.2015.08.046

52. Thompson, L. W., Kim, B., Rokers, B., & Rosenberg, A. (2023). Hierarchical computation of 3D motion across macaque areas MT and FST. *Cell Reports*, *42*(12). https://doi.org/10.1016/j.celrep.2023.113524

53. Doudlah, R., Chang, T.-Y., Thompson, L. W., Kim, B., Sunkara, A., & Rosenberg, A. (2022). Parallel processing, hierarchical transformations, and sensorimotor associations along the 'where' pathway. *eLife*, *11*, e78712. https://doi.org/10.7554/eLife.78712

54. Henze, D. A., Borhegyi, Z., Csicsvari, J., Mamiya, A., Harris, K. D., & Buzsáki, G. (2000). Intracellular Features Predicted by Extracellular Recordings in the Hippocampus In Vivo. *Journal of Neurophysiology*, *84*(1), 390–400. https://doi.org/10.1152/jn.2000.84.1.390

55. Pillow, J. W., Shlens, J., Paninski, L., Sher, A., Litke, A. M., Chichilnisky, E. J., & Simoncelli, E. P. (2008). Spatio-temporal correlations and visual signalling in a complete neuronal population. *Nature*, *454*(7207), Article 7207. https://doi.org/10.1038/nature07140

56. Pachitariu, M., Sridhar, S., Pennington, J., & Stringer, C. (2024). Spike sorting with Kilosort4. *Nature Methods*, *21*(5), 914–921. https://doi.org/10.1038/s41592-024-02232-7

57. Mizuseki, K., Sirota, A., Pastalkova, E., & Buzsáki, G. (2009). Theta Oscillations Provide Temporal Windows for Local Circuit Computation in the Entorhinal-Hippocampal Loop. *Neuron*, *64*(2), 267–280. https://doi.org/10.1016/j.neuron.2009.08.037

58. Ramaswamy, S., Courcol, J.-D., Abdellah, M., Adaszewski, S. R., Antille, N., Arsever, S., Atenekeng, G., Bilgili, A., Brukau, Y., Chalimourda, A., Chindemi, G., Delalondre, F., Dumusc, R., Eilemann, S., Gevaert, M. E., Gleeson, P., Graham, J. W., Hernando, J. B., Kanari, L., … Markram, H. (2015). The neocortical microcircuit collaboration portal: A resource for rat somatosensory cortex. *Frontiers in Neural Circuits*, *9*. https://doi.org/10.3389/fncir.2015.00044

59. Markram, H., Muller, E., Ramaswamy, S., Reimann, M. W., Abdellah, M., Sanchez, C. A., Ailamaki, A., Alonso-Nanclares, L., Antille, N., Arsever, S., Kahou, G. A. A., Berger, T. K., Bilgili, A., Buncic, N., Chalimourda, A., Chindemi, G., Courcol, J.-D., Delalondre, F., Delattre, V., … Schürmann, F. (2015). Reconstruction and Simulation of Neocortical Microcircuitry. *Cell*, *163*(2), 456–492. https://doi.org/10.1016/j.cell.2015.09.029

60. DeFelipe, J., Alonso-Nanclares, L., & Arellano, J. I. (2002). Microstructure of the neocortex: Comparative aspects. *Journal of Neurocytology*, *31*(3), 299–316. https://doi.org/10.1023/A:1024130211265

61. Fellous, J.-M., Rudolph, M., Destexhe, A., & Sejnowski, T. J. (2003). Synaptic background noise controls the input/output characteristics of single cells in an in vitro model of in vivo activity. *Neuroscience*, *122*(3), 811–829. https://doi.org/10.1016/j.neuroscience.2003.08.027

62. Destexhe, A., Rudolph, M., Fellous, J.-M., & Sejnowski, T. J. (2001). Fluctuating synaptic conductances recreate in vivo-like activity in neocortical neurons. *Neuroscience*, *107*(1), 13–24. https://doi.org/10.1016/S0306-4522(01)00344-X

63. Howell, D. C. (2013). *Statistical methods for psychology* (8th ed.). Wadsworth Cengage Learning.

64. Jain, A., Nandakumar, K., & Ross, A. (2005). Score normalization in multimodal biometric systems. *Pattern Recognition*, *38*(12), 2270–2285. https://doi.org/10.1016/j.patcog.2005.01.012

65. Guan, Z., & Wang, Y. (2023). Data-driven simulation of two-dimensional cross-correlated random fields from limited measurements using joint sparse representation. *Reliability Engineering & System Safety*, *238*, 109408. https://doi.org/10.1016/j.ress.2023.109408